Contrasting hydrogeologic regimes along strike-slip and thrust faults in the Oregon convergent margin: Evidence from the chemistry of syntectonic carbonate cements and veins

James C. Sample *Department of Geological Sciences, California State University, Long Beach, California 90840-3902*
Mary R. Reid *Department of Earth and Space Sciences, University of California, Los Angeles, California 90095-1567*

ABSTRACT

Samples of carbonate-cemented sedimentary rocks were collected during 11 *Alvin* dives in two regions along the Cascadia margin, a northern strike-slip fault zone and a southern thrust-fault zone ("second ridge"). We characterized 35 samples petrographically and chemically. Northern-area samples are dominantly sandstones; second-ridge samples are all mudstones. Vugs and high percentages of carbonate cement in the mudstones suggest that these rocks were never deeply buried. The abundance of veins and brecciation in samples from both regions attests to their proximity to faults. Northern-area cements are dominantly calcite or magnesian calcite, whereas second-ridge cements generally are more dolomitic.

Oxygen and Sr isotopic values of carbonate cements indicate the involvement of two very different fluid reservoirs during cementation. One reservoir generally has low $\delta^{18}O$, very low $\delta^{13}C$, and high $^{87}Sr/^{86}Sr$ ratios, but the other has high $\delta^{18}O$, moderately negative $\delta^{13}C$, and $^{87}Sr/^{86}Sr$ ratios lower than modern seawater values. In the northern area, diagenetic carbonates are subdivided into two populations of coupled oxygen and carbon isotopic values. Population I has $\delta^{18}O_{PDB}$ values of +3‰ to +5‰ and $\delta^{13}C_{PDB}$ values of –55‰ to –45‰. Population II has $\delta^{18}O$ values of –13‰ to –4‰ and $\delta^{13}C$ values of –25‰ to –1‰. Such common low $\delta^{18}O$ values in carbonate cements have not been observed at any other accretionary wedge. $^{87}Sr/^{86}Sr$ ratios of northern-area samples range from 0.7128 to 0.7088. Oxygen and Sr isotopic values show a correlation between increasing $^{87}Sr/^{86}Sr$ ratios and decreasing $\delta^{18}O$ values. Oxygen and carbon isotopic values of most diagenetic carbonates from the second ridge range from +3‰ to +10‰ and –55‰ to –38‰, respectively. Enrichments of ^{18}O probably result from a combination of dolomitic mineralogy, cold bottom-water temperatures, and the presence of decomposing gas hydrate in the subsurface. $^{87}Sr/^{86}Sr$ ratios of carbonates from the second ridge range from 0.7086 to 0.7091.

The geochemical signatures of diagenetic cements from the northern area suggest that fluids were derived from greater than 2 km depth, perhaps from the decollement. Prominent gullies throughout the northern area are probably underlain by strike-slip faults that provide conduits for upward fluid migration. Cements at the second ridge precipitated from shallowly derived fluids. The difference in fluid source depth is related to proximity to the fluid conduits and different orientations of minimum principal stress and resultant hydrofractures in the two fault regimes.

INTRODUCTION

At continental-margin subduction zones, sediments experience syntectonic lithification as they are accreted to continental crust (Agar, 1990; Karig, 1986; Kastner et al., 1991; Moore et al., 1991; Sample, 1990). Lithification occurs by compaction, fluid expulsion, and cementation. The chemistry of syntectonic cements and veins, and crosscutting relationships between cements, veins, and microstructures can provide a history of evolving fluid sources and deformation (Ritger et al., 1987; Sample et al., 1993; Thornburg and Suess, 1990; Vrolijk, 1987). This paper summarizes petrographic, chemical, and isotopic data for carbonate cements and microstructures in sediments collected with the Deep Sea RV *Alvin* along the Oregon segment of the Cascadia accretionary wedge (Fig. 1). The data presented are from two different tectonic regimes: a zone of prominent strike-slip faults in the north (Fig. 1) and a thrust-fault zone in the south (Fig. 2). The large number of samples containing carbonate cements with high $^{87}Sr/^{86}Sr$ ratios and low $\delta^{18}O$ values is unique to Cascadia and unprecedented in other accretionary wedges. The isotopic data from carbonate cements suggest fundamentally different fluid sources in the two different fault settings.

Tectonic Setting of Cascadia Fluid Seeps

The Cascadia accretionary wedge comprises accreted clastic sediments derived from the Columbia River and the Oregon coastal mountains, and hemipelagic sediments deposited seaward of the deformation front (Kulm and Scheidegger, 1979; Scheidegger et al., 1973) (Fig. 1). The subducting plate is mantled by up to 4 km of sediment (MacKay et al., 1992), and oceanic crust of about 9 Ma underlies the thick clastic sequence on the lower plate.

We studied samples collected from two regions of the Cascadia accretionary wedge: an area of 12 km^2 at the base of the continental slope at 45°08′N latitude (northern area, Fig. 1) and two areas totaling 1 km^2, centered on a prominent north-trending ridge at 41°40.5′N latitude (second ridge, Fig. 2). The tectonic structure of the northern area is dominated by a local, seaward-vergent (landward-dipping) frontal thrust and associated ramp anticline, and by the large, vertical Wecoma strike-slip fault transecting the deformation front in a northwest-trending direction (Fig. 1) (Goldfinger et al., 1992; MacKay et al., 1992; Sample et al., 1993; Tobin et al., 1993). A minimum of 200 m of stratigraphic section has been eroded

*E-mail: csample@csulb.edu

GSA Bulletin; January 1998; v. 110; no. 1; p. 48–59; 9 figures; 3 tables.

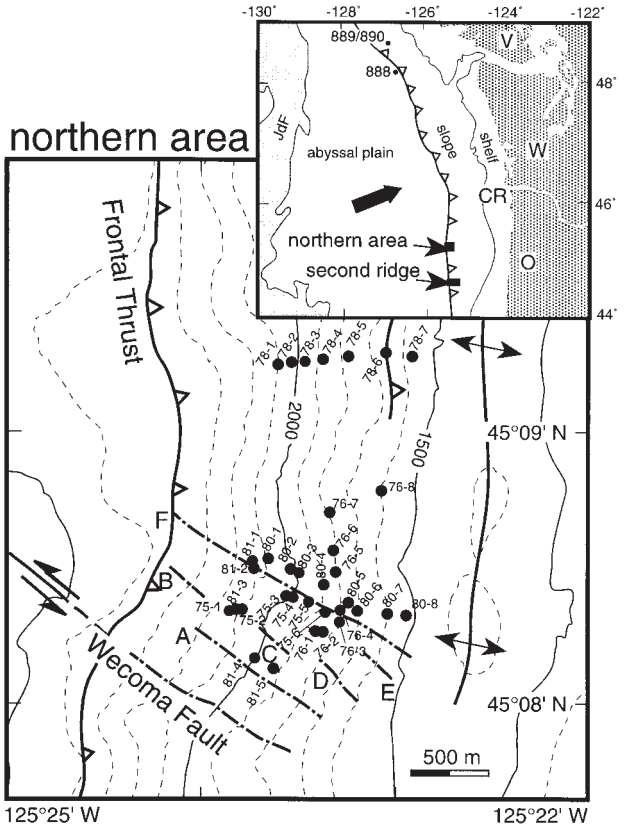

Figure 1. Tectonic map of northern area showing sample locations. Gullies (dot-dash lines) inferred to be strike-slip faults associated with Wecoma fault are labeled A through F. Black dots are sample locations with sample numbers. Inset shows general location map of the *Alvin* study sites (black rectangles); ODP Sites 888 and 889/890 also shown. Sites 891 and 892 occur within southern rectangle (Fig. 2). Wide arrow represents subduction vector of Juan de Fuca Plate beneath North American Plate (39 mm/yr) (DeMets et al., 1990). The accretionary wedge underlies the areas labeled slope and shelf. CR is location of mouth of Columbia River. V—Vancouver Island, W—Washington, O—Oregon. Oregon Coast ranges parallel shoreline.

from the seaward flank of the frontal anticline. Several large gullies, from which many of the samples were collected (A–F in Fig. 1), parallel the trend of the Wecoma fault and probably represent synthetic strike-slip faults in a main left-lateral strike-slip fault zone (Tobin et al., 1993). One transect in the northern area crossed a small, seaward-vergent thrust fault 2 km to the north of the gullied area.

To the south, the second ridge is underlain by extensive carbonate deposits forming a bioherm. The bioherm crops out at the top of the second ridge, but laterally is covered by a veneer of slope sediment (Carson et al., 1994). The carbonates are associated with a seaward-vergent thrust fault, on the west side of the second ridge, that dips 14° east beneath the second ridge (Fig. 2). The thrust appears to be an active fluid conduit, where warm fluids migrating upward have pushed up the base of the bottom-simulating reflector, thought to represent the maximum depth of gas hydrate in the sediments (Westbrook et al., 1994). Site 892 of Ocean Drilling Program (ODP) Leg 146, located about 350 m east of the exposed bioherm, penetrated 176.5 m of dominantly Miocene to Pleistocene silty clays and clayey silts (Camerlenghi et al., 1995). Two smaller thrusts form a shoulder on the eastern margin of the ridge. Three *Alvin* dives (2277, 2279, 2282) mapped the distribution of the bioherm, and one dive (2284) visited the two smaller thrusts 5 km to the east. Results from the bioherm and the eastern shoulder are discussed together because of similarities in geochemical characteristics and lithologies.

The main faults in the northern area and underlying the second ridge appear to record recent movement. The Wecoma strike-slip fault in the northern area cuts through the entire sedimentary section and the decollement, ending in oceanic basement (Goldfinger et al., 1992). The main thrust fault at the second ridge links with an east side up scarp on the sea floor (Westbrook et al., 1994). A variety of fault-related structures were recovered in cores along the thrust at Site 892, and the thrust is imaged on seismic profiles to a depth of about 0.3 km as a negative-polarity reflector (Westbrook et al., 1994). The seismic polarity reversal suggests high pore-fluid pressure in an active fluid conduit. Fluid seepage at the second ridge is evident at the sea floor from chemosynthetically supported benthic communities and large amounts of inorganic carbonate precipitates (Carson et al., 1994; Moore et al., 1991).

SAMPLE DESCRIPTIONS

The samples analyzed vary from weakly lithified to strongly lithified sandstone and mudstone. The dominant tectonic mesostructures and microstructures are veins, tension fractures, brecciation, and shear fractures with

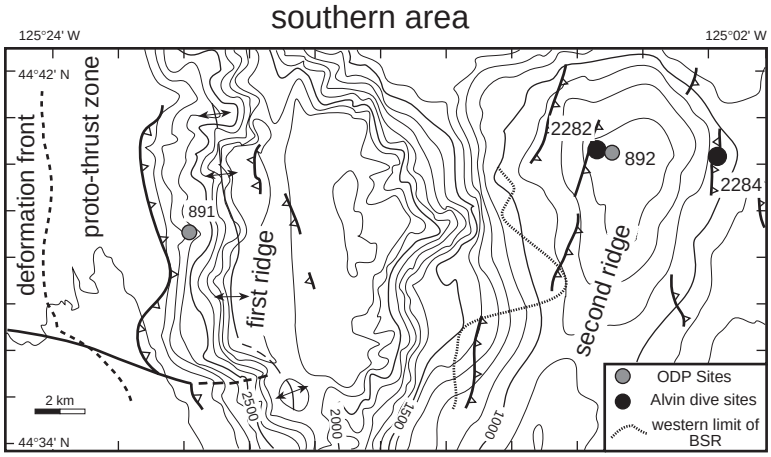

Figure 2. Tectonic map of southern area. *Alvin* dive site 2282 is near top of second ridge; dive site 2284 is on eastern flank of second ridge. Bottom simulating reflector (BSR) underlies both dive sites. Site 892 was drilled within about 100 m of *Alvin* dive site 2282.

slickensides; grain-scale cataclasis and stress solution occurs locally (Fig. 3). The samples from the northern area (*Alvin* dives 2274–2276, 2278, 2280, and 2281) comprise 23 sandstones, 4 mudstones or interlayered mudstone and siltstone, and 1 pebbly concretion; brief descriptions of chemically analyzed samples are given in Table 1. Five samples contain obvious veins or faults like those of vein networks observed in outcrops (Tobin et al., 1993). The samples collected from the second ridge (*Alvin* dives 2282 and 2284) are generally finer grained than those from the northern area (Table 1) and consist of eight mudstones, nine mudstone breccias, and a terrigenous boulder of biotite-muscovite schist (relict dropstone?). All but two of the samples contain slickensides, brecciation, or carbonate veins, attesting to the pervasive brittle deformation along the second ridge.

METHODS

All of the chemically analyzed samples were studied in thin section and by X-ray diffraction (XRD), and most were further examined for cathodoluminescence, with back-scattered electron imaging, or by electron probe microanalysis (Table 2). XRD patterns were obtained from 2° to 60° 2θ for bulk mineral analyses, and repetitively from 20° to 35° 2θ for semiquanti-

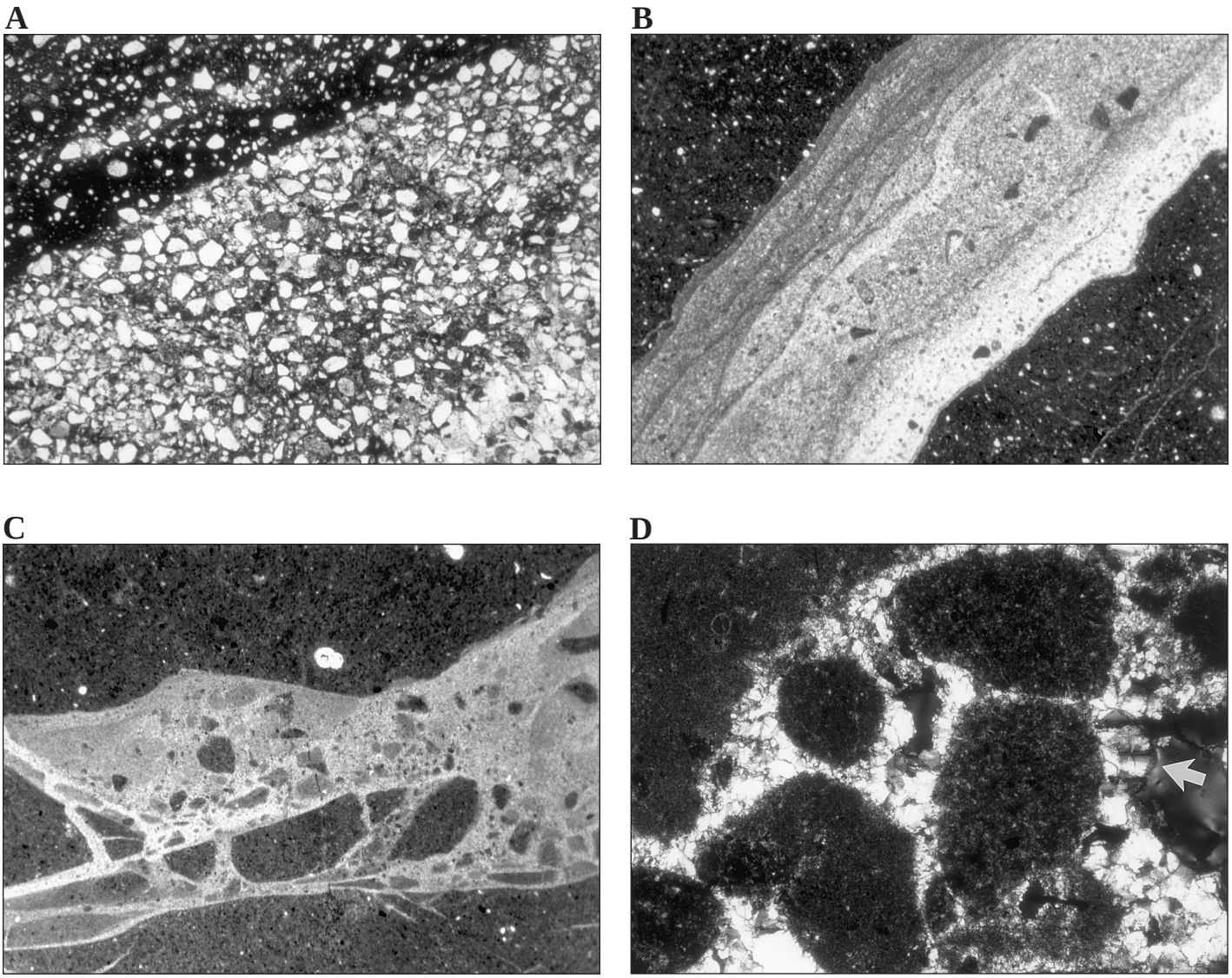

Figure 3. Photomicrographs of *Alvin* samples. Unless otherwise noted, photographs taken with plane-polarized light, length of view 5.4 mm. (A) Sample 2278–3. Light area is sandstone cemented by magnesian calcite; dark area is vein cemented by magnesian calcite and calcite, containing detrital grains (white) and more abundant, finely crystalline cement (black areas). (B) Sample 2282–2. Dolomite vein in dolostone. Banding in vein suggests multiple episodes of carbonate precipitation. Darkest areas outside of vein are finely crystalline dolomite surrounding sparse detrital grains. (C) Sample 2282–4. Breccia zone (lighter area) in carbonate crust. Within breccia zone, darkest areas are pieces of wall rock; medium and light grays are different generations of carbonate cement. (D) Sample 2282–1. Crossed-polarized light, length of view 2.7 mm. Mudstone grains (dark areas speckled with light, detrital grains) partially cemented with aragonite growing into open vugs. Arrow points to aragonite needles with radial extinction; arrow is located within a vug filled with epoxy.

TABLE 1. ROCK DESCRIPTIONS AND CEMENT TYPES OF ALVIN GRAB SAMPLES

Sample number	Lithology*	Matrix† (%)	Vein† (%)	Comments
Northern area				
2275-1	sst	MNC (27)	MNC	
2275-2	sst & sts	MC (45)		Carbonate crust
2275-4	sst & sts w/l	C (33)		Carbonate crust; local stress solution
2275-5	pb-con	MC (82)		Loose boulder, out of place
2275-6	sst	C (25)		Carbonate slab
2276-3	sst w/l	C (34)		Thin cataclasis zones
2276-4	sst	C (29)		Concretion; broken quartz and feldspar grains cemented by carbonate
2276-5	sst	C (20)	C (45)	Carbonate crust; veins; broken grains cemented by carbonate common; late stress solution
2276-6	sts	D (5)		
2276-7	sts	MC		
2278-1	sst	MNC (30)		Local broken grains, abundant crushed micas
2278-3	sst	MC (21)	MC, C (82)	Veins
2278-5	sst	D (2)		
2278-6	mst			
2280-3	sst	C, D (10)		
2280-6	sst	MC, clay(?)		Local broken grains; veins
2280-7	sst	MC, clay(?)		
2281-1c	sst w/fos	A (74)		Aragonite locally lines vugs
2281-4	sts & sst w/l	MC (57)		Small vug lined by aragonite(?)
Second ridge				
2282-1	mst	D , A (80)		Clam shell-rich; about 5% forams; aragonite fills voids and vugs
2282-2	mst	D (89)	D	Siliceous; slickensides and veins
2282-3	b-mst	CD (86)	CD	Bacterial mats(?); slickensides, vugs
2282-4	b-mst	MC	MC	Breccia fragments up to 10 mm wide in veins; slickensides
2282-5	b-mst	CD	CD	Brecciated; vugs
2282-6	b-mst	MC (85)	MC	Brecciated; four fracture generations; stress solution youngest
2282-9	mst	MC		Slickenlines
2284-1	mst	MC	MC(?)	
2284-2	mst	MC	B	Barite veins
2284-3	mst	MC(83)		About 5% forams; two vein generations
2284-4	mst	MC, CD (65)		Veins
2284-5	b-mst	CD (85)	CD	About 3% forams; two vein generations
2284-6	b-mst	MC (80)	MC	Veins
2284-7	b-mst w/l	MC (58)	MC	Veins
2284-9	mst	MC		Small vein
2284-10	mst	MC	MC	Common forams; veins

*pb-con—pebbly concretion; sst—sandstone; sts—siltstone; mst—mudstone; b-mst—mudstone breccia; w/l—layered; w/fos—fossiliferous.
†Dominant cements listed, percentages of cement in matrix or vein given in parantheses where determined; C—calcite; D—dolomite; MC—magnesian calcite; MNC—manganiferous calcite; CD—calcian dolomite (protodolomite); A—aragonite; B—barite.

TABLE 2. REPRESENTATIVE MICROPROBE ANALYSES OF CARBONATES

Sample no.:	2275-1	2278-3	2275-5	2278-3	2282-2	2284-4	2282-8
Carbonate type:	Mn-rich calcite	Mg-calcite	High Mg-calcite	Calcite vein	Dolomite vein	Ca-dolomite	Foraminifera
MgO	0.40	3.12	7.11	0.32	22.71	16.47	1.33
SrO	0.00	0.00	0.16	0.00	0.17	0.00	0.09
FeO	1.11	0.09	0.20	0.56	0.39	0.15	0.21
MnO	4.63	0.00	0.08	0.18	0.07	0.00	0.00
CaO	50.52	52.74	47.72	54.81	29.33	36.71	52.38
BaO	0.00	0.12	0.00	0.00	0.08	0.07	0.00
CO_2	43.64	44.89	45.45	43.82	48.18	46.91	42.73
Total wt%	100.30	100.96	100.72	99.69	100.93	100.31	96.74

tative characterization of carbonate abundances and compositions. (See Sample and Kopf [1995] for a more detailed description of XRD techniques used.) Quantitative mineral analyses were performed on a Cameca microprobe with a back-scattered electron detector, four crystal spectrometers, and a Kevex energy-dispersive analyzer. Standardizations used calcite (Ca), magnesite (Mg), siderite (Fe), strontianite (Sr), and garnet (Mn); the precision of analysis is ±1% relative (Table 2).

Veins were mechanically separated for oxygen and carbon isotopic analysis with a razor blade or microdrill, the latter with a spatial sampling resolution of better than 1 mm. All samples were treated with sodium hypochlorite to remove organic matter; extraction of CO_2 followed the procedure of McCrea (1950). Replicate analyses (n = 13) of a Joplin, Missouri, calcite lab standard during processing of the *Alvin* samples yielded values of $\delta^{13}C_{PDB} = -5.32‰ \pm 0.05‰$ (one standard deviation) and $\delta^{18}O_{PDB} = -24.30‰ \pm 0.33‰$. Replicate analyses of six Cascadia samples yielded a reproducibility for $\delta^{13}C$ of 0.2‰ to 0.9‰ and for $\delta^{18}O$ of 0.02‰ to 0.9‰. Sample heterogeneity probably accounts for some of the variation. The $\delta^{18}O$ values are not corrected for variations in carbonate mineralogy.

Sr isotopic analyses were performed on acid leachates of the sediments. Samples were disaggregated by gentle crushing, rinsed with micropure water, and dried, then leached with 5.0 *N* acetic acid for one hour. To evaluate possible leaching of Sr from the sediment matrix, separate fractions of five of the samples were leached for five hours in 0.1 *N* acetate buffer (method

of Apitz, 1991). Splits of all the leachates were spiked for isotope dilution determination of Rb and Sr concentrations. After drying, the leachates were redissolved in 2.5 N HCl for separation of Rb and Sr on cation exchange columns. Sr isotopic ratios were determined on a VG Instruments multicollector mass spectrometer at University of California, Los Angeles. Sr concentrations were calculated with respect to the carbonate fraction of bulk sediment determined by gravimetric methods. In addition to authigenic cements, $^{87}Sr/^{86}Sr$ ratios were measured in 16 carbonate-free, host sediment matrices (Table 3). Replicate analyses (n = 47) of NBS 987 yielded 0.710257 ± 16 (1 standard deviation). See Sample et al. (1993) for additional description of isotopic techniques.

RESULTS

Petrographic Descriptions

The diagenetic carbonates in the northern area occur as pore-filling cement, veins, and rarely linings or fillings of vugs and cavities. Cements typically compose from 10% to 40% of the sample. Some samples contain >80% carbonate, suggesting that cementation occurred before significant compaction, or that the carbonate precipitated in crusts at the sea floor with minor input of sedimentary detritus. Biogenic and detrital carbonate components are minor to absent in most of the analyzed samples, although one sample contains abundant unrecrystallized clam shell fragments (Table 1).

Framework grains in the northern area are abundant in quartz, plagioclase, mica, and amphibole, as well as rare to common altered volcanic rock fragments, pyroxene, metamorphic rock fragments, and chert. The sandstones with the least amount of carbonate cement tend to exhibit the most compaction-related structures such as crushed micas, broken grains, and a crushed or smeared clay matrix or cement. Samples 2276-4, 2276-5, and 2278-1 contain both abundant carbonate cement and compaction-related structures, however, including broken grains cemented by carbonate. Apparently early carbonate cementation in some of the sandstones protected the framework grains from further compaction during burial diagenesis, but in other samples significant carbonate cementation continued after compaction.

Veins occur in five of the samples analyzed from the northern area. In the context of this paper, "vein" refers to discrete fractures from 0.02 to 5 mm wide that are filled with material in proportions significantly different from the supporting framework of the sample (Fig. 3). Thus the term includes fractures filled with mixtures of detrital grains and cement, fractures filled with pure carbonate or other diagenetic phases, or mineralized fractures containing stylolites or evidence for cataclasis. Veins that contain mixtures of detrital grains and carbonate cement are most typical. Cement is more abundant inside than outside these veins. They contain floating grains (cement-supported) and broken grains with greater angularity and smaller grain size than the undeformed, surrounding sediment matrix.

The diagenetic carbonates in second-ridge sediments occur as pore-filling cements, breccia-zone cements, and vein fillings (Fig. 3). Cement-lined or filled vugs and cavities are more common than in the northern area, and cements from the second ridge typically compose higher percentages (58% to 89%) of the rock (Table 3). Optically identifiable detrital grains in second-ridge sediments are plagioclase, quartz, mica, glaucony, and rarely carbonate (Table 1). XRD patterns indicate that the dominant detrital grains in fine-grained samples are quartz, plagioclase, and clay minerals. Foraminifers are absent to minor in abundance (5%); locally foraminifers have recrystallized from primary Mg-calcite to dolomite.

Deformation features in second-ridge samples include veins, breccia zones, and partially open vugs or cracks (Fig. 3). Most veins are filled with microcrystalline carbonate or microsparite similar in chemical composition to the pore-filling cements (Table 1). Mineralized fractures contain relatively pure carbonate, indicating vein formation by positive dilation and mineralization from fluids, rather than infilling with cataclastically broken particles. The occurrence of isolated, intact foraminifers in some of the veins suggests some particulate flow during fracturing. Fractures or veins are locally stylolitic, indicating a history of both positive and negative dilation.

Chemistry of Diagenetic Carbonates

The dominant carbonates found as cements and veins in the dive areas are calcite, Mg-calcite, and Ca-dolomite (protodolomite), with dolomite and aragonite less abundant. Other diagenetic phases include barite, apatite, clay minerals, chlorite, and silica, but these are minor constituents and are not described further here. Representative microprobe analyses of typical carbonates are shown in Table 2, and ranges in composition are given in Figure 4. Isotopic data for the carbonates are summarized in Figures 5 and 6, and in Table 3.

The dominant carbonate phases in the northern area are Mg-calcite, calcite, and Mn-calcite (Fig. 4). In two samples (2281-1c and 2281-4), aragonite lines vugs and cavities. Cements tend to be chemically homogeneous within individual sandstones, although there is significant variation between sandstones (Fig. 4). A general increase in CaO abundance appears to correlate with decreasing grain size, but this is based on only two analyses of lithologies other than sandstones (Fig. 4). The dominant carbonate phases in the second ridge are Ca-dolomite and dolomite, with Mg-calcite common, and aragonite present in at least one sample (Fig. 4). Barite is present as dispersed cement or veins in many of the samples. Some of the dolomitic cements contain silica as a minor component (determined by semiquantitative microprobe energy-dispersive analyses), which indicates the presence of reactive silica during carbonate cementation.

There is no strong correlation between stable isotopic composition and carbonate mineralogy in samples from the northern area. Further, most of the cements analyzed are from sandstones (circles in Fig. 5). Isotopic compositions for cements from this lithology are distributed over the complete range of values, so host lithology also does not appear to influence stable isotopic values of the cements.

Stable isotopic compositions from the northern area can be divided into two main populations (Fig. 5). Population I has $\delta^{18}O$ values between +3‰ and +5‰ and $\delta^{13}C$ values between –55‰ and –45‰. These values are similar to carbonates analyzed previously from the Cascadia Basin (Kulm and Suess, 1990; Ritger et al., 1987) and, for oxygen, are mildly ^{18}O-enriched with respect to the range expected for marine carbonates precipitated at cold, bottom-water temperatures (1–2 °C). Veins from the northern area fall only into population I. Population II has $\delta^{18}O$ values between –13‰ and –4‰ and $\delta^{13}C$ values between –25‰ and –1‰. These values are more variable, and most appear to define a mixing array between the extremes of isotopic compositions. In sample 2278-3, vein-filling carbonate of population I ($\delta^{18}O$ = +3.5‰, $\delta^{13}C$ = –47.9‰) crosscuts pore-filling cement of population II ($\delta^{18}O$ = –6.4‰, $\delta^{13}C$ = –20.2‰), indicating that the latter type of cement formed earlier in the burial and deformation history of the sample. Population II carbonates were retrieved largely from the gully zone (Fig. 1; Table 3). The only gully samples with population I isotopic characteristics are 2275-2 and 2275-5; the former is a carbonate crust and the latter is a loose boulder that may have rolled down from a position farther upslope. The predominance of population II cements in the gully zone suggests a correlation between gully formation related to strike-slip faulting and strong relative ^{18}O-depletion coupled with relatively weaker ^{13}C-depletion in carbonate precipitates.

Second-ridge carbonates tend to have less variability in stable isotopic values than those from the northern area (Fig. 6). $\delta^{18}O$ values are high (+3‰ to +10‰) and most $\delta^{13}C$ values range between –55‰ and –38‰.

TABLE 3. ISOTOPE DATA OF CARBONATE CEMENTS, VEINS, AND DETRITAL GRAINS

Sample number	Location	Pop.	$\delta^{13}C_{PDB}$	$\delta^{18}O_{PDB}$	Sr* (ppm)	Rb (ppm)	Carb. (%) (est.)	$^{87}Sr/^{86}Sr^{\dagger}$ (5 *N* leach)	2σ	Carb.§ Sr (ppm)	Carb.§ Rb (ppm)	$^{87}Sr/^{86}Sr$ (buffered leach)	2σ
Northern area cements													
2275-1	Gully C	II	–12.3	–10.7			27%	0.709871	14				
2275-2	Gully C	I	–52.4	3.4									
2275-4	Gully F	II	–2.0	–10.7	69.3	0.775	33%	0.712248	10	210	2.348	0.712034	19
2275-5	Gully F	I	–54.8	5.0	605	1.565	82%	0.708974	11	738	1.909	0.709038	11
2275-6	Gully F	II	–12.8	–7.8	33.9	0.868	25%	0.709894	16	136	3.472		
2276-3	Gully F	II	–20.0	–8.3	28.1	0.452	34%	0.710483	11	83.5	1.345		
2276-4	Gully F	II	–15.1	–7.1	20.6	0.773	29%	0.710714	12	70.9	2.666		
2276-5 matrix	1.2 km north of gully F	I	–53.1	3.2									
2276-5 vein	1.2 km north of gully F	I	–51.0	3.3									
2276-6	1.3 km north of gully F	II	–1.0	–7.7									
2276-7	1.5 km north of gully F	I	–54.7	3.5									
2276-8	1.8 km north of gully F	I	–45.6	3.3									
2278-1	0.7 km west of thrust	II	–2.2	–12.9									
2278-3 matrix	0.6 km west of thrust	II	–20.2	–6.4	64.7	0.547	21%	0.709789	11	302	2.557		
2278-3 vein	0.6 km west of thrust	I	–47.9	3.5	828	0.819	82%	0.708752	8	1015	1.005		
2278-5	0.3 km west of thrust	II	–1.1	–8.1									
2278-6	Small thrust	II	–1.4	–5.5									
2280-3	Gully F	II	–1.6	–11.6	30.0	0.846	10%	0.712835	13	307	8.633		
2280-7	1.2 km north of gully F	II	–4.3	–8.4									
2281-1c	Gully F	II	–1.1	–10.5	34.8	0.337	74%	0.711392	10	47	0.455		
2281-4	Gully A	II	–25.0	–4.3	57.3	0.520	57%	0.709517	11	101	0.912	0.709439	19
Northern area detrital grains													
2275-4	Gully F				194			0.722322	13				
2275-5	Gully F				228	104.8		0.716404	10				
2275-6	Gully F				360			0.711019	10				
2276-3	Gully F				308	54.7		0.710531	8				
2276-4	Gully F				318			0.710012	10				
2278-3 vein	0.6 km west of thrust				356			0.710867	11				
2278-3 matrix	0.6 km west of thrust				344			0.711330	8				
2280-3	Gully F				322	86.5		0.712153	10				
2281-1c	Gully F				266			0.717377	10				
2281-4	Gully A				245			0.720231	10				
Second ridge cements													
2282-1	Bioherm area		–51.4	5.8									
2282-1bc	Bioherm area		–48.8	6.3									
2282-2	Bioherm area		25.9	6.2			89%						
2282-3	Bioherm area		–28.9	8.3			86%	0.708573					
2282-4 matrix	Bioherm area		–38.9	4.4									
2282-4 oldest vein	Bioherm area		–43.3	5.4									
2282-4 younger vein	Bioherm area		–45.4	6.2									
2282-5	Bioherm area		–0.6	9.2									
2282-6 matrix	Bioherm area		–38.5	6.1									
2282-6 vein	Bioherm area		–40.9	5.9									
2282-9	Bioherm area		–39.2	7.4									
2284-1	Eastern shoulder		–47.3	6.9									
2284-2 matrix	Eastern shoulder		–41.6	4.1									
2284-2 vein	Eastern shoulder		–45.7	6.7									
2284-3	Eastern shoulder		–46.5	7.0	253		83%	0.709093	4	305		0.708900	11
2284-4	Eastern shoulder		–48.1	5.6	345		65%	0.708964	5	531		0.708928	11
2284-5	Eastern shoulder		–40.7	7.3	283		85%	0.709093	5	333			
2284-6	Eastern shoulder		–54.2	6.0	442	0.717	80%	0.709045	13	553	0.896		
2284-7	Eastern shoulder		–49.9	5.4	300		58%	0.708733	4	522			
2284-9	Eastern shoulder		–1.6	5.1									
2284-10	Eastern shoulder		–32.0	3.5									
Second ridge detrital grains													
2282-3	Bioherm area				82	69.53		0.708560	9				
2284-3	Eastern shoulder				275	55.93		0.709033	9				
2284-4	Eastern shoulder				189	72.86		0.708866	9				
2284-5	Eastern shoulder				2221	67.98		0.709020	9				
2284-6	Eastern shoulder				137	73.90		0.708652	10				
2284-7	Eastern shoulder				190	62.85		0.708488	8				

Note: Pop.—population, carb.—carbonate.

*Rubidium and strontium concentrations for carbonate cements relative to whole rock, recovered by 1 hr leach in 5.0 *N* acetic acid; concentration for detrital grains is for noncarbonate fraction.

†Normalized to NBS 987 standard value of 0.710257 ± 16 (1 sd; n = 47).

§Concentration in carbonate after normalization to percent carbonate in whole rock.

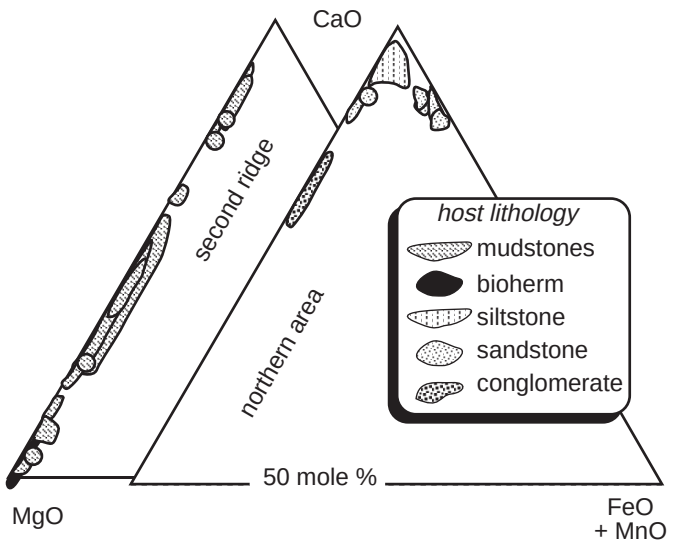

Figure 4. Ternary diagram of carbonate cement compositions from northern area and second ridge; compositions determined by microprobe analysis, shown in mole percent.

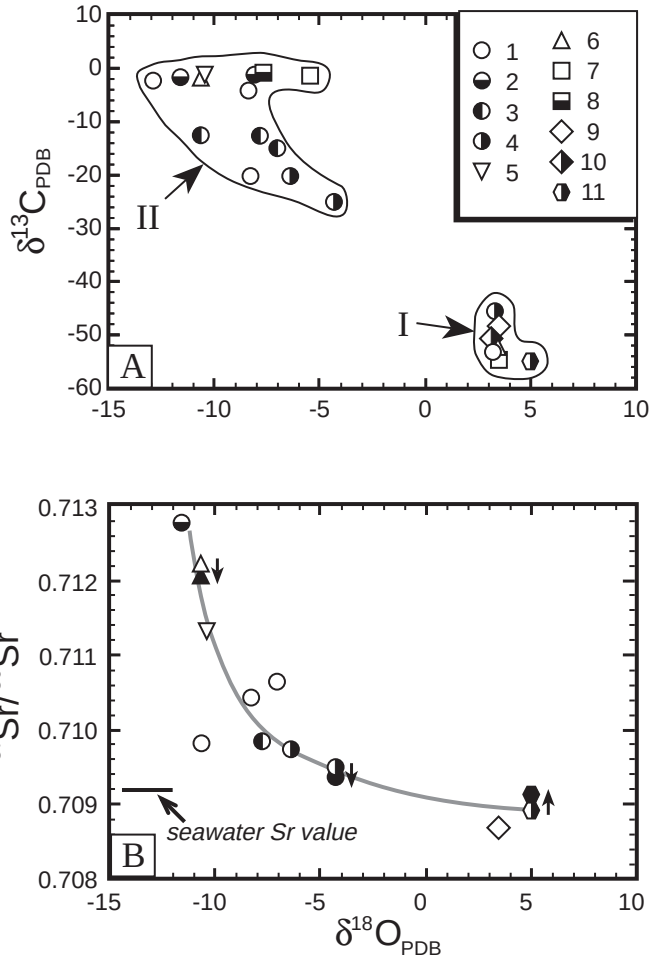

Figure 5. Isotopic data from northern area carbonate cements. (A) Stable isotopes of various lithologies and carbonate mineralogies. 1—calcite-cemented sandstone; 2—dolomite-cemented sandstone; 3—Mn-calcite–cemented sandstone; 4—Mg-calcite–cemented sandstone; 5—calcite-cemented, shelly concretion; 6—calcite-cemented, layered sandstone and siltstone; 7—calcite-cemented siltstone; 8—dolomite-cemented siltstone; 9—calcite veins; 10—Mg-calcite veins; 11—Mg-calcite–cemented pebble concretion. Where cements are heterogeneous, dominant cement is shown; for clarity, symbols are larger than precision of analyses. I refers to population I with high $\delta^{18}O$ and low $\delta^{13}C$ values. II refers to population II with higher $\delta^{13}C$ and lower $\delta^{18}O$ values. Note apparent mixing trend between the two extremes for many samples. (B) Sr and oxygen isotopes of various lithologies and carbonate mineralogies. Note apparent covariance of radiogenic $^{87}Sr/^{86}Sr$ and $\delta^{18}O$ values. Arrows show sense of change of $^{87}Sr/^{86}Sr$ from 5.0 *N*-acetic acid leach experiments (more open symbols) and 0.1 M-acetate buffer leach experiments (closed symbols). Modern $^{87}Sr/^{86}Sr$ of seawater is 0.7092.

These values are similar to population I of the northern area except that some of the $\delta^{18}O$ values of the second ridge carbonates are higher and require an explanation involving precipitation at other than simple bottom-water conditions.

The Sr isotopic composition of carbonate cements and veins also fall into two populations (Table 3; Figs. 5 and 6). Population I carbonates from the northern area and second-ridge cements have $^{87}Sr/^{86}Sr$ ratios (0.7087 to 0.7091) lower than modern seawater (0.7092) and generally have high Sr concentrations. There is little systematic correlation between $^{87}Sr/^{86}Sr$ ratios and lithology of the host rock, as is also observed for the stable isotopic data. Carbonate-free sediment matrices from the second ridge have a narrow range in Sr isotopic composition, and Sr isotopic compositions of cements and detrital grains are similar (Table 3). All of the cements for individual samples from this group, however, are slightly more radiogenic than their host matrix (Fig. 7). One sediment sample from the second ridge, unusually high in Sr (2221 ppm in sample 2284-5; concentration determination duplicated), contains cements with one of the lowest Sr concentrations in that area (333 ppm). Cements with population II oxygen isotopic characteristics have $^{87}Sr/^{86}Sr$ ratios (0.7095 to 0.7128) substantially higher and generally have Sr concentrations lower than population I by a factor of two or more. The highest $^{87}Sr/^{86}Sr$ ratio occurs in a dolomitic cement, indicating that under diagenetic conditions favorable to dolomite precipitation, the fluids present contained radiogenic Sr. Carbonate-free sediment matrices from northern-area samples yield some of the highest $^{87}Sr/^{86}Sr$ ratios (Table 3). The $^{87}Sr/^{86}Sr$ ratios of individual host sediments and their coexisting cements from the northern area differ significantly (Fig. 7). Matrices are either substantially more or slightly less radiogenic than their surrounding cements. Carbonates with high $^{87}Sr/^{86}Sr$ ratios are associated with the large gullies F, A, or C, suggesting that, as for $\delta^{18}O$, these strike-slip fault-related features have been sites of expulsion of isotopically distinct fluids compared with ambient seawater (Table 3).

The Sr isotopic distinctions between the different carbonate populations are independent of the leaching techniques used to extract the carbonate. Isotopic ratios from the buffered leach technique range from 0.00005 lower to 0.00021 higher than the 5.0 *N* acetic acid leaches (Table 3). The differences may in part reflect differential leaching of cements or minor contributions from the more radiogenic components in the matrices. Nevertheless, these differences are two to three orders of magnitude smaller than the total range in $^{87}Sr/^{86}Sr$ ratios of the samples.

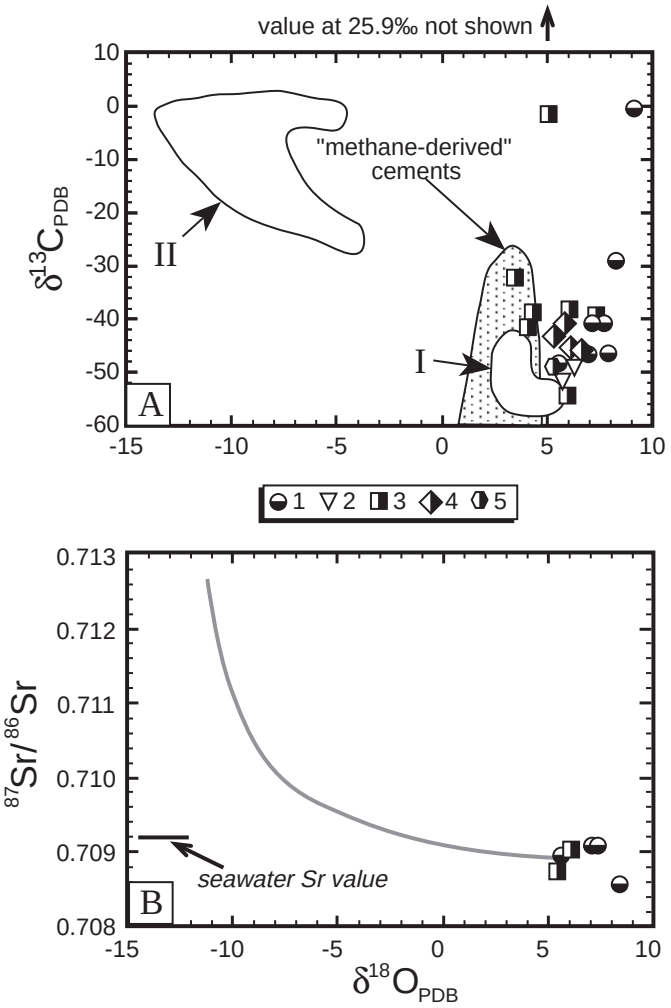

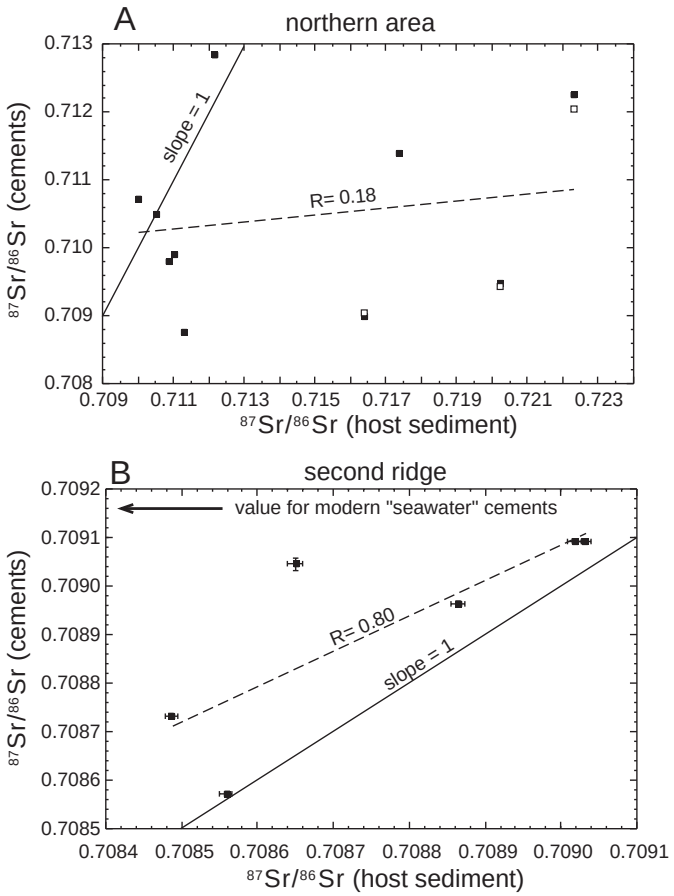

Figure 6. (A) Stable isotopic data from second ridge. 1—calcian-dolomite–cemented mudstone; 2—magnesian-calcite and aragonite-cemented fossiliferous mudstone; 3—magnesian-calcite–cemented mudstone; 4—magnesian-calcite veins; 5—magnesian-calcite–cemented crust. For clarity, symbols are substantially larger than precision of analyses. Ca-dolomites tend to be more enriched in ^{18}O than high-Mg calcite. Calcitic mudstone with an isotopic composition of $\delta^{18}O$ = +6.2‰ and $\delta^{13}C$ = +25.9‰ not shown. Scale of axes same as Fig. 5A. Northern area fields I and II shown for comparison. Field of methane-derived cements modified from Hudson (1977). (B) Sr and oxygen isotopic data from the second ridge. All analyzed samples are mudstones. Scale of axes same as Figure 5B. Mixing curve from northern area shown for reference. Results of buffered dissolution experiment not significantly different and not shown for clarity.

Figure 7. Correlation between cement and host sediment (carbonate-free) $^{87}Sr/^{86}Sr$ ratios. Correlation coefficients (R) shown for dashed line fitted to all data in each plot. 2σ analytical errors shown when larger than symbol size. (A) Northern area. In most samples, sediment host is substantially more radiogenic than authigenic carbonate (data points fall to right of line with slope = 1). Open squares represent cement values from buffered leach experiment. (B) Second ridge. All authigenic carbonate slightly more radiogenic than host sediment (data points fall to the left of line with slope = 1) and have values expected for modern seawater cements.

DISCUSSION

The isotopic systematics of the carbonate cements and veins constrain the nature of fluids present during carbonate precipitation, the potential sources of those fluids, and temperatures of precipitation. Cements in the gully area of the northern area probably derive their Sr isotopic signatures from distinctly different sources than cements from the second ridge. Significant differences between isotopic compositions of most carbonates from the northern area and the second ridge may be related to tapping of different fluid sources in tectonic systems dominated by strike-slip and thrust faults, respectively; $\delta^{18}O$ values suggest precipitation under different temperature conditions in the two regions. The following discussion begins with exploration of some general relationships between cements and fluid sources over the regions studied, progresses to an evaluation of the distinct potential fluid sources in the northern area and second ridge, and finishes by relating the dominance of the different sources in the two areas to the different tectonic regimes. The implications of carbon, oxygen, and Sr isotopes are addressed, but the focus is on the oxygen and Sr isotopic data because the probability of multicomponent mixing of carbonate reservoirs makes interpretation of carbon isotopes difficult.

Sources of Sr Isotopic Variations in Cascadia Carbonate Cements and Veins

The low $^{87}Sr/^{86}Sr$ ratios of population I cements are similar to values for Pliocene and younger foraminifers. This similarity could reflect in situ dissolution and reprecipitation of biogenic calcite during cementation, but probably does not reflect dissolution of foraminifers during sample leaching. Relatively minor amounts of foraminifers (0%–5%) are present in samples of the second-ridge, but these sediments also contain substantial authigenic cement (58%–89%). Mass balance considerations suggest that the bulk of the leachable Sr is contained within the authigenic cement. One low $^{87}Sr/^{86}Sr$ ratio was obtained from a sample (2278-3 vein) microdrilled from a vein with no observed foraminifers. Furthermore, there is no correlation between higher Sr concentrations in the leachate, as would be expected from dissolution of foraminifers (DePaolo and Ingram, 1985), and greater foraminifer abundances in the sample.

The influence of host sediment matrix on the $^{87}Sr/^{86}Sr$ ratios of the authigenic cements is evaluated in Figure 7, which compares cements to their carbonate-free, sediment matrices. In the northern area, both cements and matrices are more radiogenic than seawater. The high isotopic ratios of the relatively young, accreted sediments probably reflect the derivation of accreted Astoria-fan sediments from old crust of the continental interior (Reid and Sample, 1991). The coexistence of nonradiogenic cements with radiogenic host matrices in the area (2275-5 and 2278-3 vein), and the generally large isotopic differences between an individual cement and matrix, particularly in the northern area, indicate that cement Sr is not derived substantially from the immediate host, either by in situ diagenesis or by the acid leaching techniques used in this study.

The Sr isotopic data suggest involvement of at least two fluid reservoirs in the regions examined. The amount of Sr taken up by carbonate during precipitation is largely a function of the available Sr in the fluid and partition coefficients for different carbonate minerals (Morse, 1983, and references therein). Generally the amount of observed Sr substitution into a carbonate mineral decreases with decreasing stoichiometric Ca in the carbonate mineral. In Cascadia, Ca-normalized Sr varies by a factor of 20 (Fig. 8). Some of the higher Sr concentrations are found in dolomitic cements, indicating that concentrations of Sr in the fluid are more important than Ca-Sr exchange in influencing cement concentrations (Tables 1 and 3).

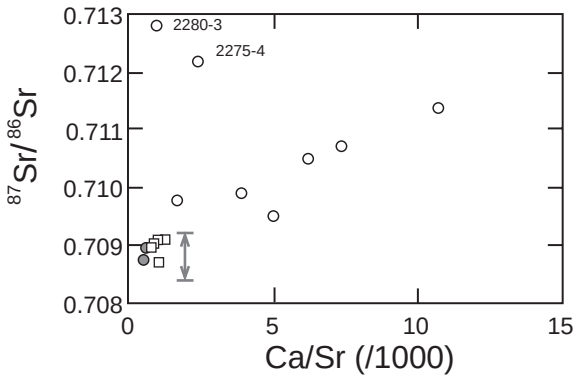

Figure 8. Plot of $^{87}Sr/^{86}Sr$ ratios vs. the reciprocal of calcium-normalized Sr concentrations for all analyzed cements. Circles are northern-area cements (gray: population I; open: population II); squares are second-ridge cements. Double-headed arrow shows range of $^{87}Sr/^{86}Sr$ for Miocene (lower arrow) to Holocene (upper arrow) foraminifers (DePaolo and Ingram, 1985).

When $^{87}Sr/^{86}Sr$ is plotted against Ca-normalized Sr (Fig. 8), the data appear to correlate despite the great distance between sample sites, the heterogeneity of mineralogy, and the possible differences in time of cementation. When all analyzed samples from the northern area are compared, there is also a correlation between increasing $^{87}Sr/^{86}Sr$ and decreasing $\delta^{18}O$ (Fig. 5). The correlation suggests that heterogeneities in population I and II cement represent mixing of two fluid types during carbonate cementation in the northern area. The curvature of this mixing array is that expected from the relative difference in Sr concentrations between the two carbonate populations. In contrast, one Sr fluid reservoir with relatively low $^{87}Sr/^{86}Sr$ ratios dominates the second-ridge samples.

Origins of Isotopic Signatures of Second-Ridge and Population I Carbonates, Northern Area

Population I samples from the northern area and all analyzed samples from the second ridge are enriched in ^{18}O and have low $^{87}Sr/^{86}Sr$ ratios, and the second-ridge carbonate cements generally have high Mg contents. The high carbonate percentages and open vugs in many of the samples from the second ridge (Fig. 3) suggest that they were never deeply buried, and possibly formed at the sea floor as crusts. The samples with moderate ^{18}O enrichments can be explained by precipitation of dolomitic mineralogies at cold bottom-water temperatures amidst locally derived fluids. The cements from the second ridge with $\delta^{18}O$ values that fall outside the maximum value typical of methane-derived cements (>~+5‰) (Curtis, 1977) probably arise from dolomitic mineralogies. A local enrichment in ^{18}O of 0.4‰ to 0.5‰ in pore fluids also was observed in the gas hydrate zone (11.4 m below sea floor [mbsf]) at ODP Leg 146 Site 892 (Kastner et al., 1995). The presence of hydrate-influenced pore fluids also could have contributed to a further increase in $\delta^{18}O$ values of the carbonate cements.

Most second-ridge carbonate cement and vein samples from Site 892 sample have isotopic values similar to those obtained in this study, but span a broader range (0.7059 to 0.7088; one value of 0.7114) (Sample and Kopf, 1995). Pore fluids from Site 892 range from 0.7077 to 0.7089 in the upper 20 m of the core (Kastner et al., 1995). The source of the Sr with these pore-fluid $^{87}Sr/^{86}Sr$ ratios may be recrystallization of Miocene or younger foraminifers, which would have high Sr concentrations (~1300 to 2800 ppm) and $^{87}Sr/^{86}Sr$ ratios of ~0.7084 to 0.7092 (Fig. 8) (DePaolo and Ingram, 1985). Sediments as old as Miocene, found within 30 m of the sea floor at Site 892 (Fourtanier, 1995), provide a shallow source of biogenic carbonate with the appropriate $^{87}Sr/^{86}Sr$ ratios. Foraminifers partially recrystallized to dolomite were observed in two second-ridge *Alvin* samples, furnishing textural evidence that foraminifers influenced the Sr reservoir of these cements.

The $\delta^{13}C$ values from the second ridge allow for many possible carbon sources. In continental-margin settings, a variety of bacterially mediated reactions dominate the isotopic signature of the carbon reservoir (Claypool and Kaplan, 1974). These reactions can produce carbon sources with a wide range in $\delta^{13}C$ values, from biogenic methane produced by fermentation (–70‰ and lower) to dissolved carbonate (up to +15‰) left as a residual from the production of biogenic methane (Irwin et al., 1977; Hudson, 1977). Production of thermogenic methane, aerobic respiration, sulfate reduction, oxidation of terrestrial or marine organic matter, and dissolution-reprecipitation of marine carbonates are processes that can generate carbon with $\delta^{13}C$ values intermediate between the two extremes given above. Although each of these processes yields $\delta^{13}C$ values with a restricted range, overlap in signatures occurs, and potential mixing between carbon sources complicates identification of unique reservoirs. Abundant biogenic methane and thermogenic hydrocarbons have been identified at depth beneath the second ridge (Whiticar et al., 1995). Oxidized biogenic methane provides a source of carbon for *Alvin* samples with $\delta^{13}C$ values lower than

–50‰. Nearly all of the other *Alvin* samples have $\delta^{13}C$ values that could result from mixing of oxidized biogenic and thermogenic methane, although mixing of oxidized biogenic methane with carbon from other sources cannot be excluded.

The carbon sources listed above cannot explain the extremely high $\delta^{13}C$ value of +25.9‰ obtained in sample 2282-2. Similar high values have been ascribed previously to carbon dioxide chemically equilibrated with methane present at high concentrations (Murata et al., 1969). Because chemical equilibration is apparently slow at low temperatures (Craig, 1953; Bottinga, 1969) such as those observed at the sea floor of the second ridge, the high $\delta^{13}C$ value reflects a carbonate formed under conditions not well understood.

Origins of Isotopic Signatures of Population II Carbonates, Northern Area

Population II carbonates, which characterize most of the cements from the northern area, are more calcitic, more depleted in ^{18}O, and have higher $^{87}Sr/^{86}Sr$ values than the second-ridge cements. We believe the Sr isotopic results accurately reflect primary variations in cements, because different leaching techniques yielded virtually identical results for five separate samples, and more important, the correlation between increasing $^{87}Sr/^{86}Sr$ and ^{18}O depletion is robust, regardless of the Sr leaching technique considered (Fig. 5).

The Sr and oxygen isotopic data of this population require a fluid source characterized by low $\delta^{18}O$ or precipitation at elevated temperature, and by radiogenic Sr. In marine coastal or shelf sedimentary sequences it is relatively common for early-formed carbonate concretions to have low $\delta^{18}O$ values (Mozley and Burns, 1993). These low values are ascribed to low-temperature rock-fluid interactions, such as alteration of volcanic matter to clay minerals, or to meteoric water flowing seaward beneath the shelf. For the northern-area samples, alteration of volcanic matter can be excluded as a source of radiogenic Sr and associated low $\delta^{18}O$ values because volcanic provenances for Cascadia sediments have $^{87}Sr/^{86}Sr$ ratios that are too low (Sample et al., 1993). Meteoric water derived from the Oregon coast is also not a likely fluid source. Although the $\delta^{18}O$ values of the population II cements are those expected for carbonates precipitated from meteoric fluids at this latitude of western North America (Craig, 1961; Dansgaard, 1964), it is unlikely that undiluted meteoric fluids could migrate through the subsurface to the base of the continental slope. Furthermore, $^{87}Sr/^{86}Sr$ ratios of the population II cements range to values greater than Columbia River water (0.71210 ± 7) (Goldstein and Jacobsen, 1987). $^{87}Sr/^{86}Sr$ ratios of meteoric waters from the Oregon Coast Ranges are not available, but the pore waters are likely to have substantially lower $^{87}Sr/^{86}Sr$ ratios because the Coast Ranges are underlain by mafic volcanic rocks with nonradiogenic, unstable volcanic matter. Flow of meteoric fluids to the continental shelf is observed in one convergent-margin environment (e.g., Dia et al., 1993), but meteoric fluids have not yet been detected in pore waters near the toe of any accretionary wedge.

The Sr and oxygen isotopic data for population II of the northern-area cements suggest a deep fluid source. The $\delta^{13}C$ values are consistent with a deep fluid source alone or mixing between deep and shallow sources. Carbonate precipitation from warm fluids derived from deep within the sedimentary section may account for the low $\delta^{18}O$ values of cements (Sample et al., 1993). In this scenario, the reservoir of deeply derived fluids contained radiogenic Sr originated from diagenesis of continentally derived minerals. Fluid temperatures calculated from the $\delta^{18}O$ values of the high-Mn cements (–13‰ to –7‰) range from 78 to 41 °C, using an estimate of $\delta^{18}O_{SMOW} = -2‰$ for the pore fluid composition. In spite of these apparent high temperatures, precipitation probably occurred at seeps or at shallow subsea-floor depths because the high-Mn cements found in population II carbonates are common only in cements formed at shallow burial depths in the zone of Mn reduction (Curtis et al., 1986). The presence of unrecrystallized clam shells and open vugs lined by primary aragonite cement in one sample (2281–1c) is characteristic of seafloor seeps (Kulm and Suess, 1990). For this sample and for the high-Mn cements, low $\delta^{18}O$ values and high $^{87}Sr/^{86}Sr$ ratios imply that the fluids migrated up to or just below the sediment-water interface without complete thermal reequilibration (cf. Sample, 1996).

Cement data from northern-area *Alvin* samples can also be compared with results from ODP Leg 146. No sites were drilled in the vicinity of the northern-area, strike-slip fault zone, but Site 891 farther south (Fig. 2) is similar in sediment and cement characteristics. Bulk sediments there are also radiogenic (0.7100 to 0.7129), but fluids are relatively nonradiogenic (0.7080 to 0.7083) (Kastner et al., 1995). The fluid Sr has not equilibrated with the in situ sediment Sr at Site 891 as also is inferred for the fluid source of northern-area carbonate cements in the strike-slip fault zone. The lack of Sr equilibration is also consistent with the observation that in the northern area, sample 2281-1c, rich in macroscopic shell fragments, does not contain cement with the same isotopic signature as the biogenic carbonate. The pore fluids are also less radiogenic than the analyzed cements at Site 891, where all cements except one have $^{87}Sr/^{86}Sr$ ratios ranging between 0.7099 and 0.7116 (Sample and Kopf, 1995). $\delta^{18}O_{SMOW}$ values of Site 891 fluids range from –0.1‰ to –1.3‰, while cements have low $\delta^{18}O_{PDB}$ values (–16.5‰ to –6.2‰), indicating that the fluids and carbonates are also out of oxygen isotopic equilibrium, even when correcting for maximum reasonable bottom-hole temperatures. This lack of oxygen isotopic equilibrium with in situ pore-fluid isotopic compositions and temperatures is also probable for northern-area cements analyzed in this study.

Fluid Flow in Thrust and Strike-Slip Faults at the Cascadia Margin

$\delta^{18}O$ and $^{87}Sr/^{86}Sr$ values of carbonate cements and veins indicate that the different fault regimes had different fluid characteristics during carbonate cementation. In the northern area the predominance of low $\delta^{18}O$ values suggests warm fluid temperatures during carbonate precipitation. Rarer, high-$\delta^{18}O$ cements also preserve evidence for colder fluids. Evidence cited earlier suggests that precipitation of both cement types occurred at or near the sea floor, during deformation and dewatering of the accreted sediments. This interpretation requires that some fluids would have to travel from significant depths, implying rapid upward migration of fluids that have little time to thermally equilibrate with shallower sediments. Strike-slip faults and related fractures underlying the gullies may have acted as conduits for upward migration of these warm fluids. The character of veins (broken grains "floating" in cement) in some of these samples suggests that the near-surface veins formed by a combination of cataclasis of the surrounding sediment matrix, particulate flow, and carbonate mineralization. The larger volume of carbonate cement in the veins than in the undeformed part of the sandstone suggests vein formation under conditions of positive dilation during faulting. These conditions would occur at low effective confining stress, due either to shallow burial or high-pore fluid pressure during faulting of well-lithified material.

The possibility of rapid upward migration of fluids can be explained in part by hydrofracture-controlled flow (Behrmann, 1991; Sibson, 1981, 1992). Sublithostatic fluid pressures are required for hydrofracture along strike-slip faults, and the fractures developed will be vertical because the minimum principal stress is horizontal (Fig. 9). Hydrofractures and fault orientations will favor efficient transport of fluids to the surface. If the strike-slip faults in the northern area are linked to the decollement, as is indicated by the seismic reflection data (Goldfinger et al., 1992; MacKay et al., 1992; Tobin et al., 1993), then fluids in the northern area may be derived from greater than the 2 km depth required by the $\delta^{18}O$ values (Fig. 9).

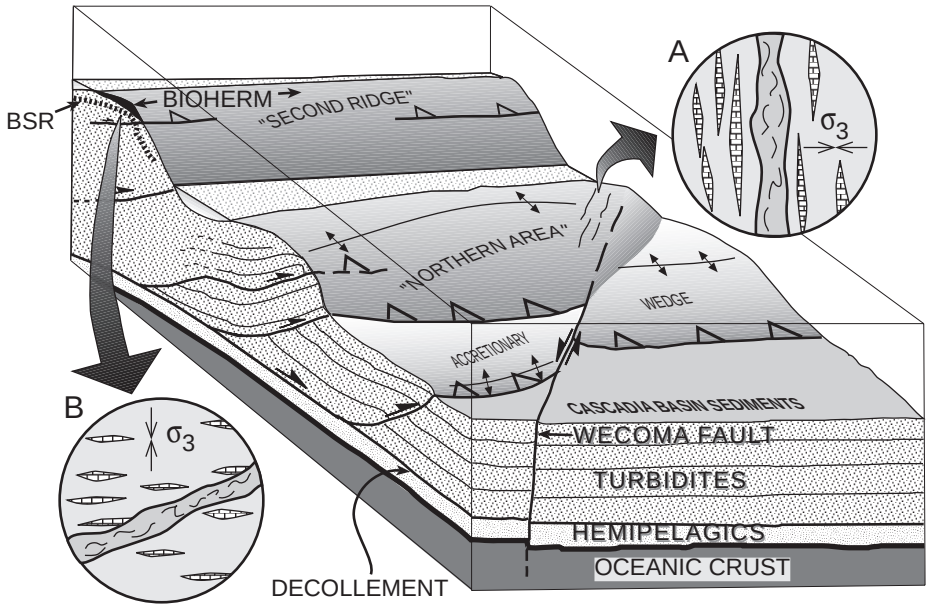

Figure 9. Composite schematic block diagram combining attributes of northern area A and second ridge B. Predicted orientation of hydrofractures and minimum principal stress shown in insets for both areas. Orientation of hydrofractures and main fault zone enhance probability of deep, warm fluids with high $^{87}Sr/^{86}Sr$ ratios reaching the surface in northern area, while shallowly equilibrated fluids will dominate at second ridge.

In contrast, the isotopic signatures of second-ridge cements to the south suggest shallow depths of origin. Fluid pressures required for hydrofracture along thrust faults must be at lithostatic or greater (Sibson, 1981). Hydrofractures will develop in a subhorizontal orientation because the minimum principal stress near thrusts is subvertical (Fig. 9; Behrmann, 1991). Longer time periods may be required for fluid pressures to build to the levels necessary for hydrofractures along thrust faults, and the orientation of the hydrofractures will be less efficient in moving fluids vertically. This will allow more time for chemical and thermal equilibration between fluids and the surrounding rock to be reached before the next hydrofracture event (Brown et al., 1994). In addition, the distance between *Alvin* sample locations, at the top of the second ridge, and the main thrust in the subsurface (~50 mbsf) may have effectively isolated the second ridge cements analyzed in this study from the influence of fluids migrating along the thrust.

CONCLUSIONS

The chemistry of Cascadia carbonate cements suggests different hydrogeological regimes: a northern area dominated by strike-slip faults wherein fluids are derived from deep levels in the accretionary wedge, and a second ridge in the south dominated by thrust faults and shallowly derived fluids. A deep origin for fluids in the northern area is suggested by coupling of high $^{87}Sr/^{86}Sr$ ratios with low $\delta^{18}O$ values. A shallow origin for fluids at the second ridge is indicated by high $\delta^{18}O$ values and $^{87}Sr/^{86}Sr$ ratios similar to recent seawater values. Although slightly warmed fluids are migrating up the thrust fault zone at the second ridge (Westbrook et al., 1994), high temperatures are not indicated by the $\delta^{18}O$ values presented here. The isotopic data suggest that carbonates forming near the top of the hanging wall are effectively isolated from the fluid regime along the main thrust fault.

ACKNOWLEDGMENTS

Funding was provided to Sample by National Science Foundation grant OCE-9020919; *Alvin* dives funded by OCE-8917705 to J. Moore. At California State University at Long Beach, E. Goldish, R. Thompson, P. Tauscher, and R. White assisted with XRD analysis; G. Lundgren assisted with the leaching experiments. At University of California, Los Angeles, stable isotope mass spectrometry was performed by D. Winter, and some thermal ionization mass spectrometry was performed by P. Holden. Discussions with M. Kastner and M. Whiticar contributed to the manuscript, but all conclusions are the responsibility of the authors. Reviews by L. D. Kulm, T. Anderson, P. Swart, and P. Knauth helped to improve the final version.

REFERENCES CITED

Agar, S. M., 1990, The interaction of fluid processes and progressive deformation during shallow level accretion: Examples from the Shimanto Belt of SW Japan: Journal of Geophysical Research, v. 95, p. 9133–9147.

Apitz, S. E., 1991, The lithification of ridge flank basal carbonates: Characterization and implications for Sr/Ca and Mg/Ca in marine chalks and limestones [Ph.D. dissert.]: Scripps Institute of Oceanography, 304 p.

Behrmann, J. H., 1991, Conditions for hydrofracture and the fluid permeability of accretionary wedges: Earth and Planetary Science Letters, v. 107, p. 550–558.

Bottinga, Y., 1969, Calculated fractionation factors for carbon and hydrogen isotope exchange in the system calcite-carbon dioxide-graphite-methane-hydrogen-water vapor: Geochimica et Cosmochimica Acta, v. 33, p. 49–64.

Brown, K. M., Bekins, B., Clennell, B., Dewhurst, D., and Westbrook, G., 1994, Heterogeneous hydrofracture development and accretionary fault dynamics: Geology, v. 22, p. 259–262.

Camerlenghi, A., Lucchi, R. G., and Rothwell, R. G., 1995, Grain-size analysis and distribution in Cascadia Margin sediments, northeastern Pacific, *in* Carson, B., Westbrook, G. K., Musgrave, R. J., and Suess, E., eds., Proceedings, Ocean Drilling Program, Scientific Results, 146, part 1: College Station, Texas, p. 3–32.

Carson, B., Seke, E., Paskevich, V., and Holmes, M. L., 1994, Fluid expulsion sites on the Cascadia accretionary prism: Mapping diagenetic deposits with processed GLORIA imagery:

Journal of Geophysical Research, v. 99, p. 11959–11970.
Claypool, G. E., and Kaplan, I. R., 1974, The origin and distribution of methane in marine sediments, *in* Kaplan, I. R., ed., Natural gases in marine sediments: New York, Plenum, p. 99–139.
Craig, H., 1953, The geochemistry of the stable carbon isotopes: Geochimica et Cosmochimica Acta, v. 3, p. 53–92.
Craig, H., 1961, Isotopic variations in meteoric waters: Science, v. 133, p. 1702–1703.
Curtis, C. D., 1977, Sedimentary geochemistry: Environments and processes dominated by involvement of an aqueous phase: Royal Society of London Philosophical Transactions ser. A, v. 286, p. 353–372.
Curtis, C. D., Coleman, M. L., and Love, L. G., 1986, Pore water evolution during sediment burial from isotopic and mineral chemistry of calcite, dolomite and siderite concretions: Geochimica et Cosmochimica Acta, v. 50, p. 2321–2334.
Dansgaard, W., 1964, Stable isotopes in precipitation: Tellus, v. 16, p. 436–468.
DeMets, C., Gordon, R. G., Argus, D. F., and Stein, S., 1990, Current plate motions: Geophysical Journal International, v. 101, p. 425–478.
DePaolo, D. J., and Ingram, B. L., 1985, High-resolution stratigraphy with strontium isotopes: Science, v. 227, p. 938–941.
Dia, A. N., Aquilina, L., Boulegue, J., Bourgois, J., Suess, E., and Torres, M., 1993, Origin of fluids and related barite deposits at vent sites along the Peru convergent margin: Geology, v. 21, p. 1099–1102.
Fourtanier, E., 1995. Neogene diatom biostratigraphy of Site 892, Cascadia margin, *in* Carson, B., Westbrook, G. K., Musgrave, R. J., and Suess, E., eds., Proceedings, Ocean Drilling Program, Scientific Results, 146, part 1: College Station, Texas, p. 79–116.
Goldfinger, C., Kulm, L. D., Yeats, R. S., Appelgate, B., MacKay, M. E., and Moore, G. F., 1992, Transverse structural trends along the Oregon convergent margin: Implications for Cascadia earthquake potential and crustal rotations: Geology, v. 20, p. 141–144.
Goldstein, S. J., and Jacobsen, S. B., 1987, The Nd and Sr isotopic systematics of river-water dissolved material: Implications for the sources of Nd and Sr in seawater: Chemical Geology, v. 66, p. 245–272.
Hudson, J. D., 1977, Stable isotopes and limestone lithification: Quarterly Journal of the Geological Society of London, v. 133, p. 637–660.
Irwin, H., Coleman, M., Curtis, C. D., 1977, Isotopic evidence for several sources of carbonate and distinctive diagenetic processes in organic-rich Kimmeridgian sediments: Nature, v. 269, p. 209–213.
Karig, D. E., 1986, Physical properties and mechanical state of accreted sediments in the Nankai Trough, southwest Japan arc, *in* Moore, J. C., ed., Structural fabrics in Deep Sea Drilling Project cores from forearcs, Geological Society of America Memoir 166, p. 117–133.
Kastner, M., Elderfield, H., and Martin, J. B., 1991, Fluids in convergent margins: What do we know about their composition, origin, role in diagenesis and importance for oceanic chemical fluxes: Royal Society of London Philosophical Transactions, ser. A, v. 335, p. 275–288.
Kastner, M., Sample, J., Whiticar, M., and Hovland, M., 1995, Geochemical evidence for fluid flow and diagenesis at the Cascadia convergent margin, i*n* Westbrook, G., Carson, B., Musgrave, R. J., and Suess, E., eds., Proceedings, Ocean Drilling Program, Scientific Results, 146, part 1: College Station, Texas, p. 375–384.
Kulm, L. D., and Scheidegger, K. F., 1979, Quaternary sedimentation on the tectonically active Oregon continental slope, *in* Doyle, L. J., and Pilkey, O. H., eds., Geology of continental slopes: Society of Economic Paleontologists and Mineralogists Special Publication, p. 247–263.
Kulm, L. D., and Suess, E., 1990, Relationship between carbonate deposits and fluid venting: Oregon accretionary prism: Journal of Geophysical Research, v. 95, p. 8899–8916.
MacKay, M. E., Moore, G. F., Cochrane, G. R., Moore, J. C., and Kulm, L. D., 1992, Landward vergence and oblique structural trends in the Oregon margin accretionary prism: Implications and effect on fluid flow: Earth and Planetary Science Letters, v. 109, p. 477–491.
McCrea, J. M., 1950, On the isotopic chemistry of carbonates and the paleotemperature scale: Journal of Chemical Physics, v. 18, p. 849–857.
Moore, J. C., Brown, K. M., Horath, F., Cochrane, G., Mackay, M., and Moore, G., 1991, Plumbing accretionary prisms: Effects of permeability variations: Royal Society of London Philosophical Transactions, ser. A, v. 335, p. 275–288.
Morse, J. W., 1983, The kinetics of calcium carbonate dissolution and precipitation, *in* Reeder, R. J., ed., Carbonates: Mineralogy and chemistry: Washington, D.C., Mineralogical Society of America, p. 227–264.
Mozley, P. S., and Burns, S. J., 1993, Oxygen and carbon isotopic composition of marine carbonate concretions: An overview: Journal of Sedimentary Petrology, v. 63, p. 73–83.
Murata, K. J., Friedman, I., and Madsen, B. M., 1969, Isotopic composition of diagenetic carbonates in marine Miocene formations of California and Oregon: U.S. Geological Professional Paper 614-B, p. B1–B24.
Reid, M. R., and Sample, J. C., 1991, Seawater and continental sources for syn-tectonic diagenetic carbonates in the Cascadia accretionary wedge, Oregon: Sr and Nd isotope evidence: Geological Society of America Abstracts with Programs, v. 23, p. A366–A367.
Ritger, S., Carson, B., and Suess, E., 1987, Methane-derived authigenic carbonates formed by subduction-induced pore-water expulsion along the Oregon/Washington margin: Geological Society of America Bulletin, v. 98, p. 147–156.
Sample, J. C., 1990, The effect of carbonate cementation of underthrust sediments on deformation styles during underplating: Journal of Geophysical Research, v. 95, p. 9111–9122.
Sample, J. C., 1996, Isotopic evidence from authigenic carbonates for rapid upward flow in accretionary wedges: Geology, v. 24, p. 897–900.
Sample, J. C., and Kopf, A., 1995, Geochemistry of syntectonic carbonate cements and veins from the Oregon margin (ODP Leg 146): Implications for the hydrogeologic evolution of the accretionary wedge, *in* Carson, B., Westbrook, G., Musgrave, R., and Suess, E., eds., Proceedings, Ocean Drilling Program, Scientific Results, 146, part 1: College Station, Texas, p. 137–148.
Sample, J. C., Reid, M. R., Tobin, H. J., and Moore, J. C., 1993, Carbonate cements indicate channeled fluid flow along a zone of vertical faults at the deformation front of the Cascadia accretionary wedge: Geology, v. 21, p. 507–510.
Scheidegger, K. F., Kulm, L. D., and Piper, D. J. W., 1973, Heavy mineralogy of unconsolidated sands in northeastern Pacific sediments: Leg 18, Deep Sea Drilling Project, *in* Kulm, L. D., and von Huene, R., eds., Initial reports of the Deep Sea Drilling Project, Volume 18: Washington, D.C., U.S. Government Printing Office, p. 877–888.
Sibson, R. H., 1981, Controls on low-stress hydrofracture dilatancy in thrust, wrench and normal fault terrains: Nature, v. 289, p. 665–667.
Sibson, R. H., 1992, Implications of fault-valve behaviour for rupture nucleation and recurrence: Tectonophysics, v. 211, p. 283–293.
Thornburg, T. M., and Suess, E., 1990, Carbonate cementation of granular and fracture porosity: Implications for the Cenozoic hydrologic development of the Peru continental margin, *in* Suess, E., and von Huene, R., eds., Proceedings, Ocean Drilling Program, Scientific Results, 146, part 1: College Station, Texas, p. 95–110.
Tobin, H. J., Moore, J. C., MacKay, M. E., Orange, D. L., and Kulm, L. D., 1993, Fluid flow along a strike-slip fault at the toe of the Oregon accretionary prism: Implications for the geometry of frontal accretion: Geological Society of America Bulletin, v. 105, p. 569–582.
Vrolijk, P., 1987, Tectonically driven fluid flow in the Kodiak accretionary complex, Alaska: Geology, v. 15, p. 466–469.
Westbrook, G. K., Carson, B., and Musgrave, R., et al., 1994, Proceedings, Ocean Drilling Program, Scientific Results, 146, part 1: College Station, Texas, 611 p.
Whiticar, M. J., Hovland, M., Kastner, M., and Sample, J. C., 1995, Organic geochemistry of gases, fluids, and hydrates at the Cascadia accretionary margin, *in* Carson, B., Westbrook, G. K., Musgrave, R. J., and Suess, E., eds., Proceedings, Ocean Drilling Program, Scientific Results, 146, part 1: College Station, Texas, p. 385–398.

MANUSCRIPT RECEIVED BY THE SOCIETY JUNE 3, 1996
REVISED MANUSCRIPT RECEIVED MAY 5, 1997
MANUSCRIPT ACCEPTED MAY 15, 1997

Printed in U.S.A.